PROCEEDINGS, 41st Workshop on Geothermal Reservoir Engineering
Stanford University, Stanford, California, February 22-24, 2016
SGP-TR-209

Inverse Numerical Modeling of Rantau Dedap Geothermal Field after Six Exploration Wells

Alexandre Bacquet, Alfianto Perdana Putra, Grimur Bjornsson, Andri Arnaldsson

Supreme Energy, Menara Sentraya 23rd floor, Jl. Iskandarsyah Raya No.1A, Jakarta Selatan 12160, Indonesia

alexandre-bacquet@supreme-energy.com

Keywords: numerical simulation, inverse modeling, iTOUGH2, Sumatra.

ABSTRACT

In 2014-2015, six deep exploration wells were drilled in Rantau Dedap geothermal greenfield located in South Sumatra, Indonesia. The exploration program being completed, Supreme Energy Rantau Dedap consortium in collaboration with Warm Artic Ehf built and calibrated the numerical model of the reservoir in a very time efficient way to carry out the reserves assessment of the field. A large contribution to this efficiency has come from the use of the iTOUGH2 program which automatically calibrates a TOUGH2 numerical model against most of the observed data collected over the exploration period by solving the inverse problem.

According to the conceptual model that depicts a large reservoir strongly controlled by faults at depth, the model follows a single porosity approach where the near vertical faults are explicitly defined at their true locations and with their own properties. The model has limited thickness and extent, tight lateral boundaries, and can therefore be regarded as conservative. 36 parameters were inverted for at maximum, most of them being the horizontal and vertical permeabilities of the faults and rocks defined in the model, and the characteristics (rate and possibly enthalpy) of the deep upflow and surface outflow.

The final results of the inversion are very consistent with the conceptual model, with a high enthalpy deep upflow connected to a wide and permeable shallow outflow through a few high permeability faults hosted at depth by a tight matrix. The resulting match of the observed data is satisfactory, except for two wells on the northwestern side whose temperature reversals are not reproduced properly by the model. This misfit highlights the necessity to improve the faults description in the West and Southwest parts of the field by acquiring more structural data.

1. INTRODUCTION

In 2014-2015, Supreme Energy, Engie and Marubeni carried out the exploration of Rantau Dedap geothermal greenfield located in South Sumatra, Indonesia, by drilling and testing six deep exploration wells. In order to proceed to the Front End Engineering Design (FEED) of the future power plant, the production capacity of the field and the forecast of the production parameters (mainly the mass flow and enthalpy) over the 30 years of contracted operation had to be determined. Such an assessment requires to take into consideration the various physical (and possibly chemical) mechanisms that come into play in the subsurface part of the living geothermal system, to find the optimum production and re-injection scheme that will maximize the capacity of the field at lower cost, and to predict the reservoir behavior over time under such a scheme to ensure the capacity is maintained.

Coupled heat and mass transfer in the highly heterogeneous environment of a geothermal reservoir involves complex physical processes and requires a tool with modeling capabilities for non-isothermal, multiphase and sometimes multicomponent problems, discretized in space and time. With the advent of digital computers, geothermal simulators were able to provide a numerical solution of such problems, and the use of numerical reservoir modeling in planning and managing the development of geothermal fields has become standard practice for about 30 years now (O'Sullivan et al., 2000).

Inverse modeling is a technique to estimate the hydrogeologic and thermal properties of a geothermal reservoir by automatically matching the output of a numerical model to data collected in the field. iTOUGH2 is an optimization code that allows such an automated calibration of the model (Finsterle et al., 1997), by minimizing the differences between the observed and simulated field responses. However, iTOUGH2 inversions are computationally intensive because the forward problem (the calculation of state variables using TOUGH2 simulator) must be solved several times to evaluate the misfit between the observed and simulated data, and to numerically calculate sensitivity coefficients (Finsterle and Pruess, 1999).

By collaborating with Warm Artic Ehf in Iceland and Vatnaskil Consulting Engineers, whose team members are highly experienced in inverse modeling, Supreme Energy Rantau Dedap (SERD) benefitted from the experience and the computational environment needed to use iTOUGH2. Following the methodology previously developed by the authors (Bjornsson and Arnaldsson, 2015), the two teams worked in very close collaboration and managed to build the numerical model of Rantau Dedap reservoir and to assess its production capacity in a very time efficient way. This model is the scope of the present paper.

2. CONCEPTUAL MODEL

The concession of Rantau Dedap geothermal greenfield covers approximately 35,000 ha and is situated at an elevation ranging from 1000 to 2600 masl on a complex andesitic volcanic terrain. The prospect is located on the northern side of the Great Sumatra Fault (GSF) and within the Semendo Caldera in West Sumatra (Figure 1), and contains several volcanic centers dominated by the one of

Bukit Besar. Geological mapping and LiDar imagery were found very useful in detecting the structural features that consist mostly of NW-SE striking faults and a near perpendicular set of younger NE-SW strike slip faults expected to be more permeable.

Numerous surface thermal manifestations including fumaroles, steaming grounds and hot springs are reported in Rantau Dedap, with steam-generated activity at high elevations in the South, and outflow of chloride water to hot springs at lower elevations in the North. These thermal features seem strongly controlled by the faults detected, in particular the NE-SW ones.

Both the chemistry and distribution of the chloride springs located along the SE-NW axis between Cawang Tengah Atas and Cawang Tengah define a broad (at least 3 km wide) Southwest to Northeast outflow. Fumaroles gas chemistry also indicates the presence of a heat source around Bukit Besar summit, with a possible steam cap in this area. Additional heat sources elongated West-East between Bukit Besar and Anak Gunung could exist and feed the system as well. No thermal activity exists in the Indikat Besar River, which is considered as the northern boundary of the field, even though the conductor body revealed from MT surveys extends much further North.

Except for this, the interpretation of the MT data leads to a delineation of the resource consistent with the previous observations: an almost continuous conductive layer over a large part of the field representing the smectite clay cap, local domings of this conductor along the Bukit Besar – Anak Gunung axis that could correlate with one or several heat sources, and the signature of an outflow in the Northeast with the conductor becoming gradually deeper and thicker in this direction. However, the survey did not extend further West of Luang Basung fumarole and the reservoir boundary in this direction is still uncertain.

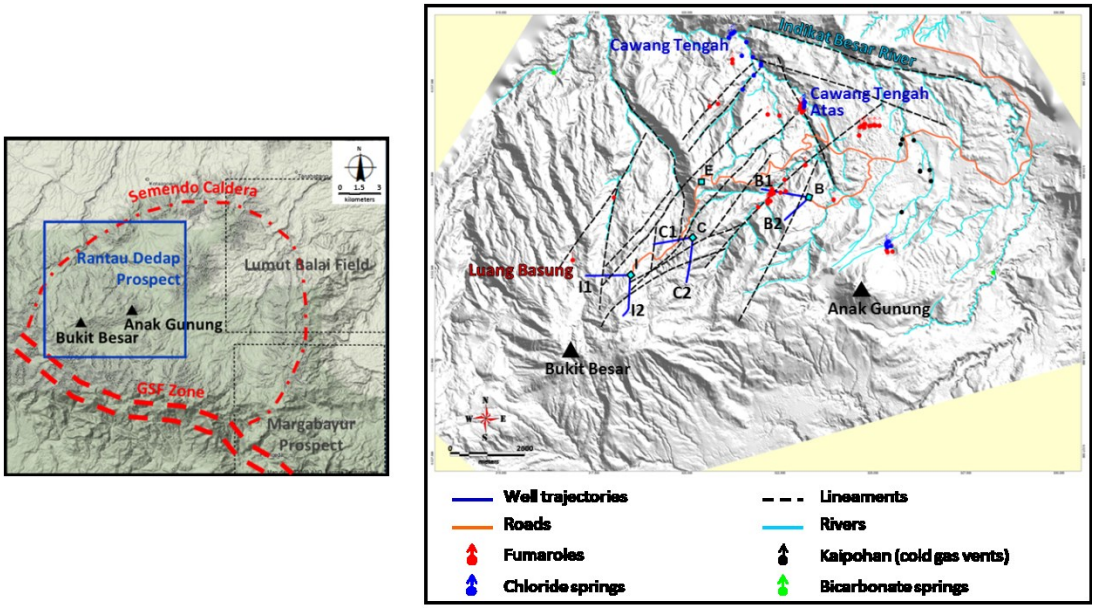

Figure 1: Regional (left) and local (right) maps of Rantau Dedap prospect

By cross correlating the initial pressure and temperature distributions interpreted from the testing of the six exploration wells (Figure 2) with most other existing surface exploration and wells data, a conceptual reservoir model of a large SW-NE elongated and fracture dominated high temperature reservoir has emerged (Figure 3). In this model, the hot upflow zone of the reservoir is seen as a diagonal plume of more than 300 ºC water coming in from depth from the Southwest of well RD-I2. This fluid ascends to about 800 to 1200 masl upper reservoir layer where the flow direction becomes horizontal and toward the Northeast. Initially the reservoir temperature in this layer is near 230 ºC, but levels off to 210-220 ºC farther North. A thin 30-60 m thick steam cap is inferred from the downhole pressure and temperature data, detected at about 1000 masl in RD-I1, 1100 masl in RD-C1, and possibly at about 1170 masl in RD-B1. From the temperature data, a fairly flat top of reservoir can be inferred at 1200 masl.

The general northeasterly flow of 210-230 ºC fluid originated from the upflow zone near RD-I2 finds escape to surface as neutral chloride springs of Cawang Tengah Atas in the North, at about 1350 masl elevation, which is actually the initial water table of the reservoir, apparently controlling the whole pressure regime. The shallow reservoir pressure seems to be equilibrated at about 1000 masl while the temperature appears relatively uniform, suggesting good horizontal extent and permeability there. The deep reservoir pressure, on the other hand, is dominated by a pressure low in RD-I2, suggesting higher anisotropy at depth. This pressure low stimulates a deep horizontal recharge from the Northeast to the upflow area. Such a deep and horizontal inflow from the boundary also explains the temperature reversals observed at the bottom of each well, except for RD-I2 which seems to be tapping the upflow of the system. In particular, a significant temperature reversal is observed in the bottom of RD-I1 (less than 1.5 km apart from RD-I2) and supports the concept of a more anisotropic reservoir at depth, strongly controlled by near-vertical Northeast fractures separated by very low permeability matrix.

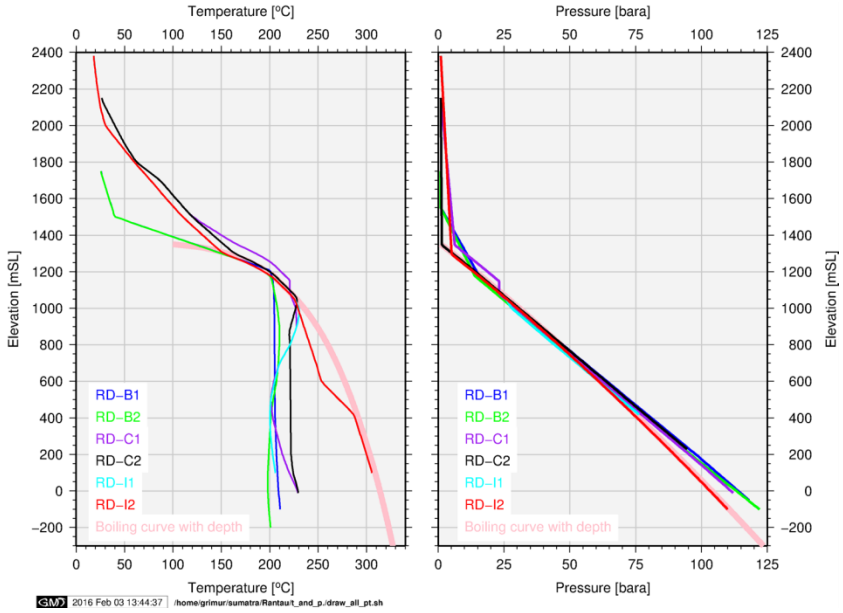

Figure 2: Interpreted initial pressure (right) and temperature (left) profiles of the six exploration wells

The downhole pressure and temperature data suggest therefore a geothermal system with a mushroom-shaped temperature distribution initiated from RD-I2 area (Figure 3), supporting the concept of an upper reservoir of relatively good horizontal permeability channeling water from the hot upflow toward the Northeast. At depth, the reservoir is strongly controlled by the near vertical NE-SW faults and should be modeled as such. These faults convey vertically the hot water from the upflow to the upper part of the reservoir, and channel horizontally colder water from the Northeast boundary toward the low pressure upflow zone.

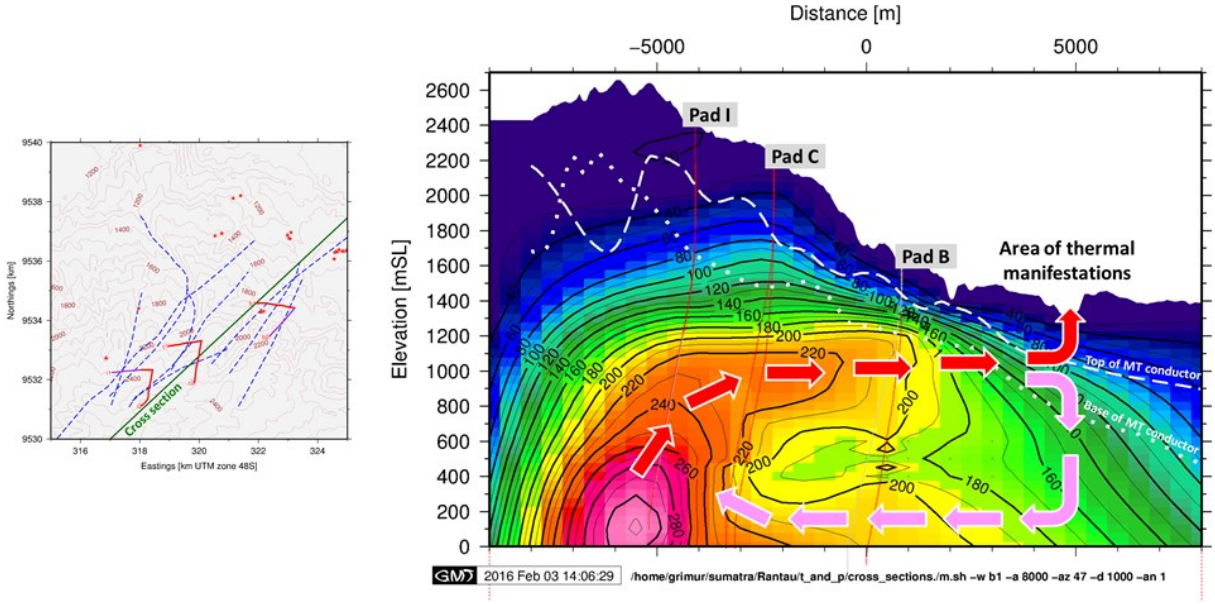

Figure 3: SW-NE cross section of Rantau Dedap reservoir with temperature contouring from wells data

3. MODEL STRUCTURE

3.1 Grid structure

Rantau Dedap numerical model covers a 50x50 km area. The model coverage was made extensive in order to avoid boundary effects that may arise with the pressure drawdown associated with the field production, and also to be able to set a linear vertical temperature gradient for the outside boundaries elements. This gradient was set at 60 ºC/km based on surveys and data available in the region.

The model mesh was built with irregular elements using the AMESH software of the Lawrence Berkeley National Laboratory. The outer part of the model is fairly coarse while the inner part, which covers the core of the geothermal system, is refined with regular hexagons of about 200 m height (Figure 4). This type of refinement leads to a mesh of 1658 elements per layer.

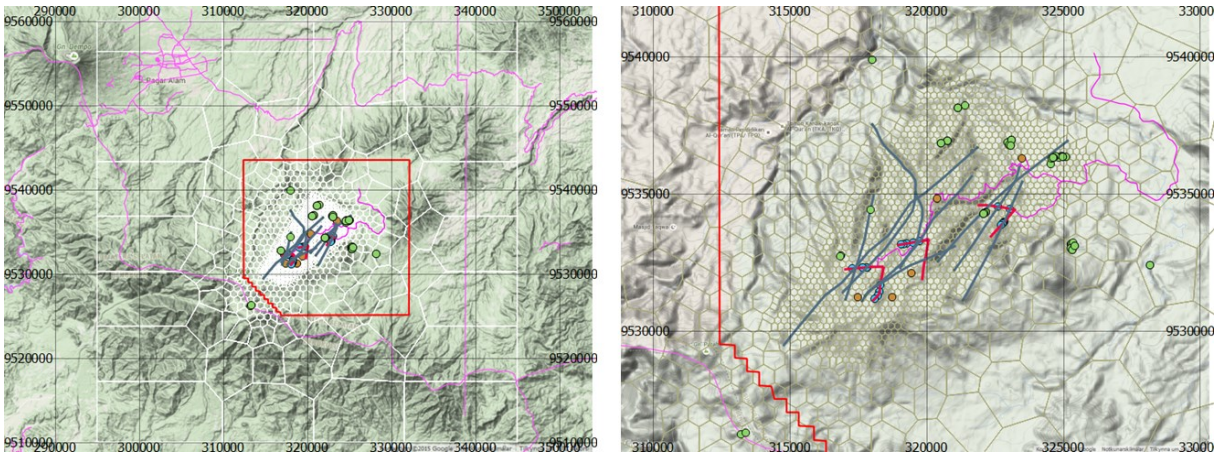

Figure 4: Full extent of the model mesh (left) and its inner part (right), with wells (red), feed zones (blue dots), thermal manifestations (green), lineaments (blue lines), and access roads (purple)

A total of 15 horizontal layers were introduced, ranging from 1800 to -600 masl (Figure 5). Even though the top of reservoir is believed to be fairly flat (as discussed already) and tightly sealed by the clay cap (consistent chemical and hydrological signature points towards minimum dilution with shallower and colder fluids), the first 2 layers A and B were built to reproduce the topography and handle the possible perched aquifer that may reside in the mountain peak. In these two layers, the elements that were out of the mountain (i.e. that were air basically) were assigned a zero vertical permeability and a constant pressure and temperature reflecting the ambient air conditions (thus, water only equation of state is sufficient for this model).

The third layer C represents the cap rock and is 200 m thick, from 1200 to 1400 masl. The layers below are refined as they represent the reservoir. The 6 first ones are each 50 m thick only to accurately reproduce the steam cap distribution and its possible expansion during field development. The following 5 ones are gradually thicker, from 100 to 400 m. The final one is also 400 m thick but is only used to set the bottom boundary conditions (defined as inactive, i.e. with constant pressure and temperature).

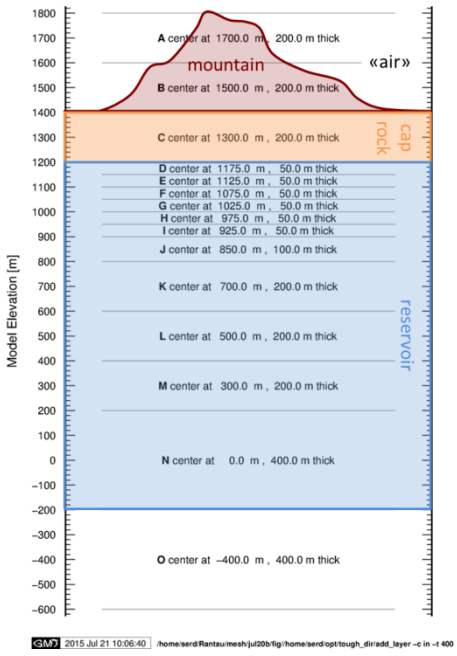

Figure 5: Vertical layering of the numerical model

Therefore, the deepest active layer N is centered at 0 masl, which is the maximum depth reached by the exploration wells. Although the vertical fluid convection of the geothermal system appears to extend deeper (RD-I2 showing no sign of temperature reversal), it was decided to stay on the conservative side and to limit the extent of the model to this known depth.

Under this configuration, the total number of elements in the model is 24870, including 4190 inactive ones (fixed pressure and temperature). This number appears reasonable to practically perform inverse modeling with parallel computing (discussed later).

3.2 Explicit fault modeling

As it was previously discussed, the geothermal system of Rantau Dedap is strongly controlled by discrete faults and needs to be modeled accordingly. With the computer power available today, it is possible to work with fine enough meshes suitable to explicitly define the main faults of the system, namely to use a single porosity modeling approach. Therefore, the near vertical faults that were described with high or medium level of confidence by SERD Subsurface team were defined explicitly in the model mesh with their own elements and own properties as their true locations can be traced fairly accurately thanks to the flexibility of the hexagons (Figure 6). However, one should be aware that this approach requires to provide accurate and extensive mapping of geological structures.

In addition, care is needed as the fault zones may not be as wide as the model hexagons. The resulting overestimation of the stored heat in the faults can be compensated mathematically by lowering the heat capacity of these fault rocks. In this model, sensitivity runs prove that the impact of this was limited, therefore this point is not developed further in this paper.

3.3 Rock type definition

The reservoir extent in the model is mostly constrained by the distribution of the surface thermal manifestations and the conservative interpretation of the MT data (with limited extent of the reservoir toward the West). Within the reservoir, faults are defined explicitly, each of them having a specific rock type. In between, two rock types are defined based on the existing wells lithological data: from layer N to K, the matrix is made of rhyolite only, while from layer J to D, the matrix is made of both rhyolite and tertiary sediments (the distribution of these two rock types being based on the well-to-well lithology correlation). As an example, Figure 6 shows the different rock types attributed in layer H, each of them having a different color relatively to its horizontal permeability (red being high, green being low). This figure is actually the result of the calibration process and will be discussed in more details later.

Outside of the reservoir, a specific rock type is attributed and represents the tight rocks surrounding Rantau Dedap geothermal system. On top of it, another rock type represents the clay cap and another one defines the mountain peak (or the air) above.

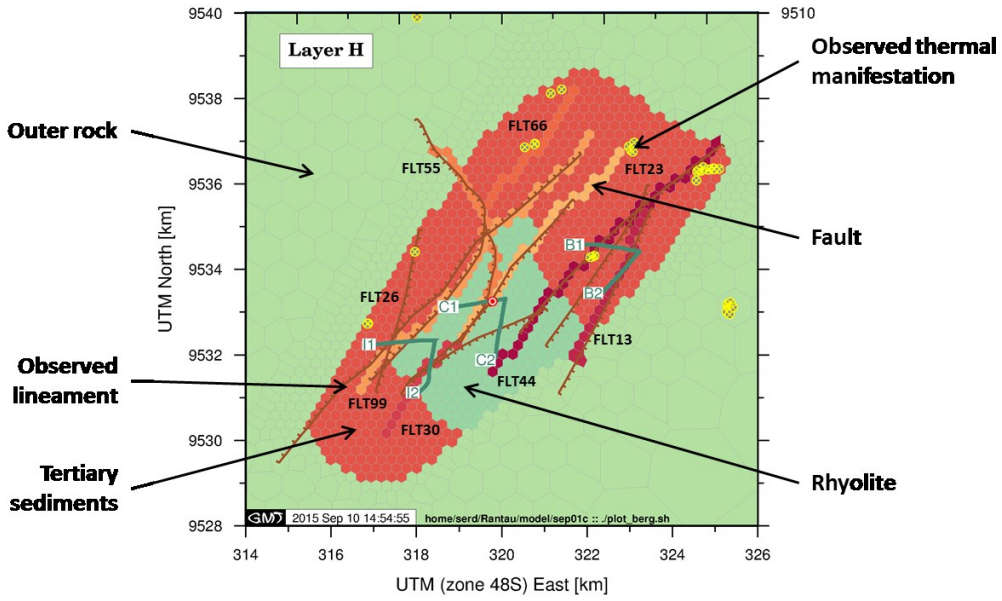

Figure 6: Rock typing and explicit fault modeling

3.4 Boundary conditions

The boundary conditions are dictated by the static pressure and temperature profiles of the exploration wells (Figure 2). Layer C, which represents the clay cap and is centered at 1300 masl, holds the flat water table of the reservoir, spotted at 1350 masl. The elements which are overlaid by the "air" elements in layer B are therefore set as inactive with a constant temperature of 28 ºC and a constant pressure of 5 bara, and are assigned a very low horizontal permeability. The other elements in the center remain active, still with a very low horizontal permeability. On top of these elements, the mountain elements of layer B are active while the ones of layer A are inactive at 1 bara and 20 ºC. These mountain elements have a low horizontal permeability. However, the vertical permeabilities of the mountain and clay cap elements are left open for inversion to check if the inverse calibration will push these to zero and thereby comply with the field observations (i.e. no infiltration from the perched aquifer into the geothermal reservoir).

The outermost rim of the model elements starts in layer C and is set inactive at the same constant temperature of 28 ºC and constant pressure of 5 bara. Below layer C, the outermost elements within each layer are active but act as a constant temperature boundary (imitated numerically by setting the heat capacity of these rim elements as infinity, i.e. 1E+50 J/kg/°C). Their temperature with depth is set to follow the 60°C/km regional thermal gradient, while their pressures adjust to the hydrological equilibrium. The volume of these outermost elements is big enough to accommodate some recharge (limited by the low permeability of these outer rocks) into the reservoir in response to the pressure drawdown associated with the field production.

The base layer O is specified as a heat flow boundary only (zero mass flow). This is achieved by setting all elements in the layer as inactive, specifying its pressure in hydrological equilibrium with the 60°C/km thermal gradient of the side boundaries, and set its vertical permeability to zero. A temperature contouring map (Figure 7) was built based on the exploration wells data (in particular the temperature anomaly at the bottom of RD-I1), the assumed location of the upflow (discussed later), the assumed shape and structure of the geothermal reservoir and the boundary conditions. This map was then used to assign a fixed temperature to each element of the base layer. By modeling the bottom boundary this way, no overestimation of mass influx is made (especially when pressure drawdown occurs with production) and the upflow of the system is easier to calibrate as a simple source of hot water.

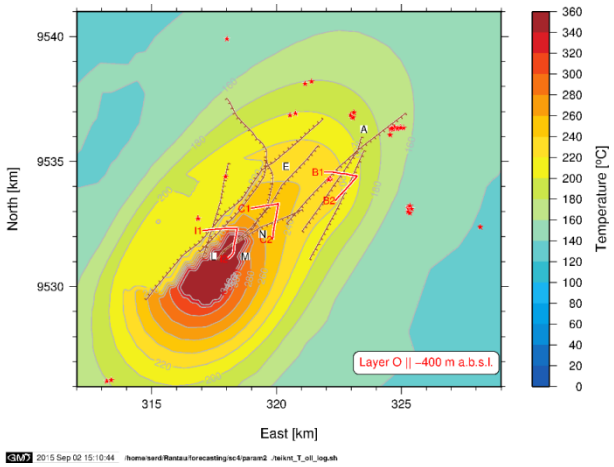

Figure 7: Temperature map used for the model base layer

The accuracy of the temperature map of the model basement was found to be important into achieving a good match of the model results with the measured data. This is particularly true away from the upflow, where heat flow is governed mostly by conduction. For example, no acceptable match of RD-I1 initial temperature could be achieved if the temperature anomaly of the bottom of this well was not reflected in this map.

In addition, it can be noted that since layer O is a heat flow boundary only, the thickness of the layer here is not known. To adjust the strength of the heat conduction mechanism, it is simpler to make the heat conductivity of the layer as a model parameter to be inverted for.

3.5 Sources and sinks

Prior to calibrating the numerical model, it is necessary to specify where a hot and deep inflow is recharging the reservoir, and where mass can escape. For Rantau Dedap, the inflow needs to be close to RD-I2, which is interpreted as tapping the upflow. Its exact location is not known at the moment, but for various reasons (doming of the conductor body from MT data, temperature trend decreasing from Southwest to Northeast, interpretation of the geochemistry data, ...) this upflow zone seems most appropriately located 1-2 km to the Southwest of the total depth coordinates of RD-I2. Therefore, two sources of hot water were introduced in permeable fault elements of layer N to represent the deep hot upflow rising from the large-scale convective system. The mass rate and enthalpy of these two sources were left open for inversion.

The mass being recharged deep into the model has then to escape, ideally near the location of the surface thermal manifestations. Therefore, four mass sinks were introduced in elements corresponding to the thermal manifestations in the Northeast and West of the field (Figure 6), in the uppermost reservoir layer of the model (layer D). These sinks are put on deliverability, i.e. mass will escape through them proportionally to the difference between the model pressure and a constant downstream pressure specified for those sinks. The rate is furthermore dictated by the productivity index of these elements, which is left open for inversion.

In addition, steam is allowed to escape from layers D and E around pad I area to imitate steam loss to surface and into the overlaying groundwater in the mountain. This energy loss actually served to cool the shallow part of the model and thereby better capture the observed temperatures. This sink is controlled by steam enthalpy mass extraction, which strength is left open for inversion as well.

4. INVERSE CALIBRATION

4.1 Objective function and optimization algorithm

Inverse modeling consists in estimating model parameters from measurements of the system response made at discrete point in space and time. The parameters to be estimated are selected coefficients in the governing flow equations, such as hydrogeologic and thermal properties, initial and boundary conditions, ... For a given set of parameters, the objective function measures the misfit between the measured data and the model results. The standard mathematical expression of the objective function is the weighted least squares, which is the sum of the residuals (the absolute value of the difference between the measured data and the model results) weighted by the inverse of the measurements error:

$$S = \sum_{i=1}^{m} \frac{\left(z_i^* - z_i\right)^2}{\sigma_{z_i}^2} \quad (1)$$

where S is the objective function, z_i^* is the measured data and z_i the model result for observation number *i*, σ_{z_i} is the standard deviation of the measured data z_i^*, and *m* is the total number of observations available as discrete values in space and time.

The best-estimate set of parameters is therefore the one that minimizes the objective function. The search for the minimum of the objective function occurs in a *n*-dimensional space, *n* being the number of parameters that are inverted for. Consequently, one should be careful when choosing the parameters to be inverted for since it will impact the topology of the objective function (whether it presents a global minimum, or multiple local minima, non-linearity, discontinuity, ...) and the efficiency of the minimization algorithm.

All these algorithms consist in solving multiple times the so-called forward problem, i.e. the simulation of fluid and heat flow through the porous media with a given parameters set (using TOUGH2 reservoir simulator). This is managed by an iterative process, called the inversion problem, assessing at the end of each step the sensitivity of the last parameters set on the objective function in order to find the optimal change (in direction and in length) of the whole parameters set that will reduce the objective function at the next step. The initial values of the parameters set can be either the best educated guess from the current knowledge of the reservoir, or the results of previous inversions, or a combination of both. To reach a faster convergence of the forward runs, it is usually better to allow the automatic update of the initial values at the beginning of each iteration.

Most of these forward runs are independent from each other and can therefore be carried out in parallel via a cluster of PCs run under the Linux operation system (Finsterle and Pruess, 1999). This parallelization is mandatory to make the method practical, the whole iterative process being completed in about 12 hours typically by doing some 500 to 1000 forward runs.

During the calibration process, different algorithms can be used alternately in order to try to reduce the objective function even more. For example, the Levenberg-Marquardt minimization algorithm is known to perform well. However, this algorithm can remain trapped in a local minimum. In this case, evaluating a subset or the whole set of parameters over their entire range of possible values (Grid Search algorithm) may allow to quit this local minimum. More information can be found in iTOUGH2 user's guide (Finsterle, 2007).

In conclusion, inverse modeling makes a very valuable contribution toward the solution of the model calibration problem. Nevertheless, one shall be aware that the minimum found by a given algorithm is not necessarily the global minimum of the objective function, and that even the best-estimate set of parameters still contains the uncertainty on the measured data, and most of all, on the whole conceptual model that is being considered.

4.2 Observations

The quantity of available observations is key to a robust inversion. In order to apply inverse modeling to build the reservoir model of Rantau Dedap after six wells only, it was necessary to make the most of all the available data sets:

- Initial temperatures in all wells, one value per layer for each well, valid at time 0 (natural state). As the interpretation of the static temperature profile of each well was properly constrained, a standard deviation of 5 °C only was attributed for each temperature observation (except in layers A and B, where it is infinite).
- Initial pressures in all wells, one value per layer for each well, valid at time 0 (natural state). Again, as the interpretation of the static pressure profile was properly constrained, a standard deviation of 5 bar was attributed for each pressure observation (except in layers A and B, where it is infinite).
- Enthalpy histories of all wells recorded during the production testing period. For each well, the whole history was considered and changes of enthalpy under throttling conditions (RD-I1 case) or because of sudden boiling of the deeper feed zones (RD-I2 case) were attempted to be matched. This involves an acute interpretation of the well testing data (particularly the Pressure Temperature Spinner surveys) since the respective contributions of the feed zones were changing under such circumstances. Consequently, great care was brought to input the correct mass flows of each feed zone in the production history of the model. The quality of the production data monitoring being high (with regular Tracer Flow Test surveys), the standard deviation for each enthalpy observation is 100 kJ/kg.
- Pressure drawdowns at each feed zone of all wells during the production periods. This is a perilous exercise since it is never easy to measure a pressure drawdown in a well that can be representative for a reservoir model: the true initial reservoir pressure is difficult to estimate precisely, the wellbore flowing pressure is known only from a few Pressure Temperature Spinner surveys that can be affected by measuring errors, near wellbore effects (downflow, …), and are not necessarily comparable to the average block pressure calculated by the simulator (which does not take into account the pressure drop associated with the skin of the well). Therefore, it is usually better to remain simple and to attribute one single value of drawdown (the best estimate based on the different pressure profiles under shut-in and flowing conditions) for each feed zone of a given well, constant in time. To compensate this approximation, a standard deviation of 3 bar was attributed for each drawdown observation (this is similar or higher than most of the measured drawdown).
- Downhole pressure changes recorded continuously with capillary tubing in observation wells RD-I1 and RD-C1 during the interference test. The analysis of these data shows very minor interference (nearly 0 bar) in these wells during the various production tests of neighboring wells. Therefore, these pressure change observations are set to zero during the whole recording period, with a standard deviation of 3 bar as well (this could be reduced).

These data comprise 190 data sets used by the minimization algorithm of iTOUGH2. Some of them only exist at one time step during the calibration (initial pressures and temperatures), while others subsist for many time steps (production data such as enthalpy and pressure drawdown) and thereby can contribute significantly to the misfit assessment of the iTOUGH2 objective function. In total, the number of observations (m in formula (1)) is 1397, consisting of 2*81 for steady state temperatures and pressures in wells, 191 for enthalpy measurements of production wells and 1044 for pressure drawdown in production and observation wells.

Considerable work was put into generalizing the export of production monitoring files of 30 minutes record density into averaged daily flow, properly distributed between the respective feed zones of each well (in accordance with the interpretation of the well testing data as already discussed). In addition, special care was required to assign the downhole observations to the correct elements of the model (i.e. to correlate the wells trajectory with the correct elements centers in each layer). This is of particular importance when faults are defined explicitly since the modeled pressures and temperatures might be very different in two adjacent elements if one is a permeable fault and the other a tight rhyolite for example.

4.3 Parameters to be inverted for

As discussed earlier, the choice of the parameters to be inverted for impacts significantly the efficiency and robustness of the minimization algorithm used in the inversion process. Therefore, one should be cautious in the choice of these parameters, their number and their respective allowable range. These are usually changed during the course of the whole calibration process, reducing the number of the parameters to be inverted for or widening the allowable range of a given parameter for example.

In this case study, 36 model parameters were inverted for at maximum. Most of them are the horizontal and/or vertical permeabilities of the model faults and rocks (29 parameters), the mass and enthalpy of the deep upflow zone, the productivity index or rate of the sinks (hot springs and fumaroles), the thermal conductivity of the base layer, and finally the relative permeability cut-off values for steam and brine in the Corey curves. All the other model parameters were based on an educated guess and remained fixed during the whole calibration process.

4.4 Management of the faults and rocks distribution

Before running the inversion over the whole set of parameters, a general good practice is to start the process of inverse calibration by inverting for the horizontal permeability of each fault independently, i.e. to complete separately x inversion runs with only one parameter to be inverted for, x being the number of faults defined explicitly in the model (in this case study, x is equal to 8). This is carried out relatively quickly since all these inversions are single parameter ones (and they can be run on the different PCs of the cluster at the same time). This first step allows to detect the most sensitive faults and possibly decide to gather some of them under the same rock type (thus decreasing the number of parameters to be inverted for) or to leave them independent from each other (each one ending up with a specific permeability value).

During the course of the calibration, the permeabilities of many of the faults defined in the model turned out to be very sensitive. This implies first that the feed zones defined along each well trajectory were assigned to a model element of enough permeability, namely a fault. In the case of Rantau Dedap, the feed zones interpreted from well testing data corresponded to the interpreted faults trace in a quite consistent way. Therefore most of them were already defined in faults elements of the model. A few were not and required to modify slightly the extent of some of the model faults.

Secondly, it quickly became evident that some of the observation data could not be matched with the initial faults outline based on the available geological data. Therefore, as can be seen on Figure 6, some of the initial faults traces that were considered initially (marked as “Observed lineaments” on the figure) had to be removed or extended. Of particular importance are the extension of the very high permeability fault FLT44 linking RD-C2 to RD-B1, and the extension toward the upflow of fault FLT30 hit by RD-I2. In addition, well testing data indicate that RD-I2 might be producing from two distinct faults, meaning that a fault might be missing from the initial faults outline. To mitigate this, fault FLT30 was split into two parts, allowing two different permeability values in the upper and in the lower parts of the fault. This remark highlights the necessity to improve the geological mapping in this part of the field.

These considerations are also true for the distribution of the different rock types filling the space between the faults (rhyolite and tertiary sediments in the case of Rantau Dedap model). A fine-tuning of the initial distribution of these rocks is often required in several layers of the model (especially when only a few wells data are available) in order to achieve a reasonable match to the measured data.

This management of the faults and rocks distribution is part of a trial-and-error process that involves to run the inversion process several times, analyzing its results and modifying slightly the model structure each time. This has to be done manually by the modelers based on their understanding of the reservoir behavior since the inversion process does not optimize the faults location automatically. In total, the construction of the model and its inverse calibration process were completed in one and a half months.

5. RESULTS OF THE INVERSE CALIBRATION PROCESS

5.1 Rocks in the best model

Nineteen rock types are specified in the model. All are assigned 10% porosity not being calibrated for. The thermal conductivity is fixed at 2.1 W/m/°C, except for the base layer for which the inversion set its value at 10 W/m/°C (this value having no real physical meaning since it depends on the thickness arbitrarily set for the base layer as discussed earlier). Their heat capacity is always that of igneous rock, i.e. 850 kJ/kg/°C, except for the outermost rim elements which were assigned an infinite heat capacity to set constant temperature conditions at the model outer margins. Rock density is fixed at 2650 kg/m^3 for all rock types.

For the mountain and clay cap elements of the model, the vertical permeabilities have been determined by the inversion process. Interestingly they ended up at about 1E-4 and 1E-5 mD only respectively. This demonstrates that the automated inverse calibration also seeks to seal the deeper model from possible perched aquifer in the higher mountain.

For the outer elements bridging the volume between the outer rim and the inner mesh (Figure 6), both horizontal and vertical permeabilities were inverted for. They resulted in the order of 1 mD in horizontal and 0.05 mD in vertical. Together with the limited thickness chosen for the reservoir model, this tightness of the lateral boundaries contributes to limit boundary pressure support during future production and allows to regard this model as conservative.

In the inner mesh of the model, a large part of the upper reservoir (layers D to J) consists of tertiary sediments, which resulted to be amongst the most sensitive rock types in the model calibration. The inversion process set their horizontal permeability quite high at 310 mD, their vertical permeability being only 3 mD however. It was found that the inversion process was regularly pushing the horizontal permeability of this rock type at the upper limit of the allowed range. This is believed to be caused by the very good homogeneity of pressures and temperatures in the upper part of the reservoir and by the very limited pressure interferences observed during the well testing campaign. However, with no well data to support high permeability values in these areas, the horizontal permeability of the tertiary sediments in the model was capped to 310 mD to avoid being overoptimistic. In the rest of the upper part and in the whole bottom part (layers K to N) of the reservoir, the matrix elements are made of rhyolite, whose permeabilities were found by inversion at 1.3 mD in horizontal and 0.1 mD in vertical, which is very consistent with the conceptual model.

For each of the 8 faults that were defined explicitly in the model, both the horizontal and vertical permeabilities were found by inversion. The main fault of the system is fault FLT44 connecting RD-B1 to RD-C2 (in dark purple on Figure 6), with about 2.5 D horizontal permeability and 10 mD vertical permeability. This high permeability is dictated by the very low pressure drawdown observed at these wells during discharge tests. Fault FLT13 and the upper part of fault FLT30 (split into two parts as discussed earlier) are very permeable as well, with about 1 D in horizontal, and about 20 and 170 mD in vertical respectively. Again, these high permeabilities are dictated by the very low pressure drawdown observed in RD-B2 and at the upper feed zone of RD-I2 respectively.

On the lower permeability side, fault FLT99 hit by RD-I1 is given about 60 mD in horizontal and 180 mD in vertical. Similarly, the lower part of fault FLT30 is only 5 mD in horizontal while 120 mD in vertical. Here the inversion tries to match the low temperature anomaly at the bottom of RD-I1 by enhancing the vertical convection from the upflow and thus limiting the horizontal propagation of heat. In addition, fault FLT26 (the Northeast striking fault splaying out from RD-I1) was found at about 5 mD in horizontal and was taken out of the upper model to avoid it to act as a barrier inside the 310 mD tertiary sediments. This fault however exists in the deep model (layers K to N), where tight rhyolites dominate the inner wellfield.

Therefore, with the tertiary sediments comprising less than 400 m of the 1400 m of reservoir thickness (from layers D to N), about 70% of the geothermal reservoir model volume is strictly speaking fracture dominated and hosted by the 1.3 mD tight rhyolites. Long term production from these faults will either tap mass horizontally from the outer model, or vertically from the upper model where the permeable tertiary sediments reside.

5.2 Sources and sinks in the best model

For the upflow, the calibration process found a total rate of 40 kg/s at 2570 kJ/kg enthalpy. These two parameters were found to be amongst the most sensitive ones for the model calibration. This high enthalpy is indeed required to create the pressure low in the upflow area (by reducing the density of the fluid column there) that triggers the deep cold water returns from the outer boundaries. This is also supported by the boiling of the deep feed zones of RD-I2 during production tests (the initial temperature in the bottom of RD-I2 sitting on the saturation curve on Figure 2) and might reflect the possible supercritical conditions of the roots of the geothermal system.

The mass sinks introduced in the North (springs) and in pad I area (steam loss) were found at a rate of 37 and 4 kg/s respectively. This compares well with a heat loss survey that identified 15 kg/s brine and 6 kg/s steam coming to surface (keeping in mind that some thermal manifestations may still be unexplored and that minor thermal seepages may be consumed into the regional groundwater flow).

5.3 Natural state and production history matching

5.3.1 Initial pressures and temperatures

The interpreted initial pressure and temperature profiles of the six wells in Rantau Dedap comprise important and dominating dataset in the numerical model calibration. The match of the model results (squares) with the interpreted data (lines) is presented in Figure 8 with the model layering reported as yellow and white strips.

As can be seen, pressure and temperature profiles in the wells are properly captured by the model (from layers C to N) except for the deep temperature reversal in RD-C1 and RD-I1. The most probable reason for this is a missing structural feature that would actually link the northwestern boundary to the upflow area. This should allow some peripheral cold recharge at depth triggered by the pressure low of the upflow. This highlights again the necessity to acquire a better knowledge of the faults distribution in this part of the field.

Furthermore, a mismatch can be observed in the top part of the reservoir in wells RD-C2, RD-I1 and RD-I2 where the model pressures and temperatures indicate the presence of a significant steam cap. In these wells, testing data were interpreted conservatively with no or a thin steam cap (thinner than the layers thickness). However, even though these field data do not prove the existence of a steam cap as depicted by the model, they are not against it neither. In addition, the conceptual model that is considered here assumes the existence of such a steam cap. Therefore, the pressures and temperatures match in the top part of the reservoir is regarded satisfactory.

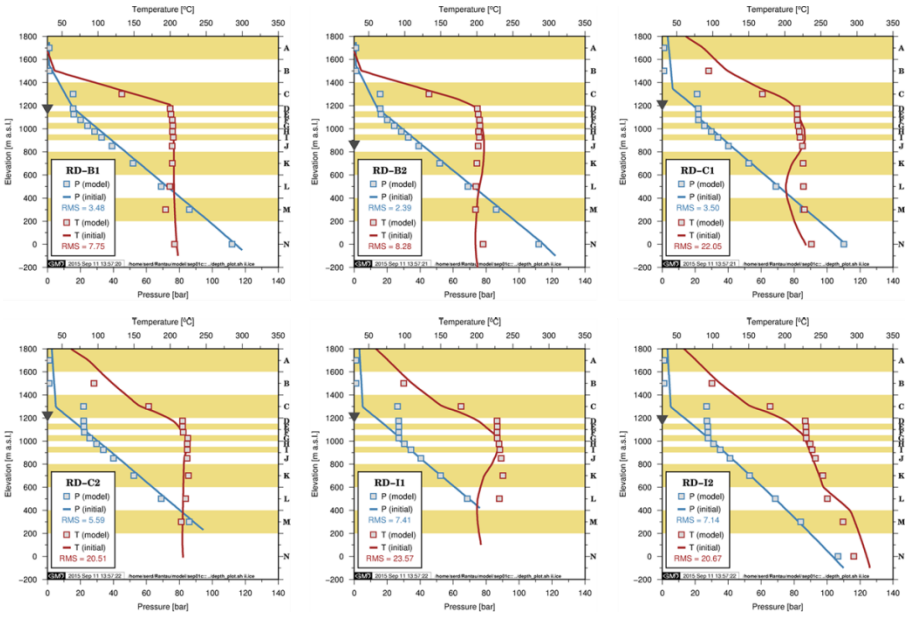

Figure 8: Initial pressures (blue) and temperatures (red) match at the six exploration wells (model as squares and field data as lines)

The planar temperature distribution in the upper part (layer E) and the lower part (layer N) of the reservoir is shown in Figure 9, with black arrows showing the flow direction and magnitude (proportional to the arrows length).

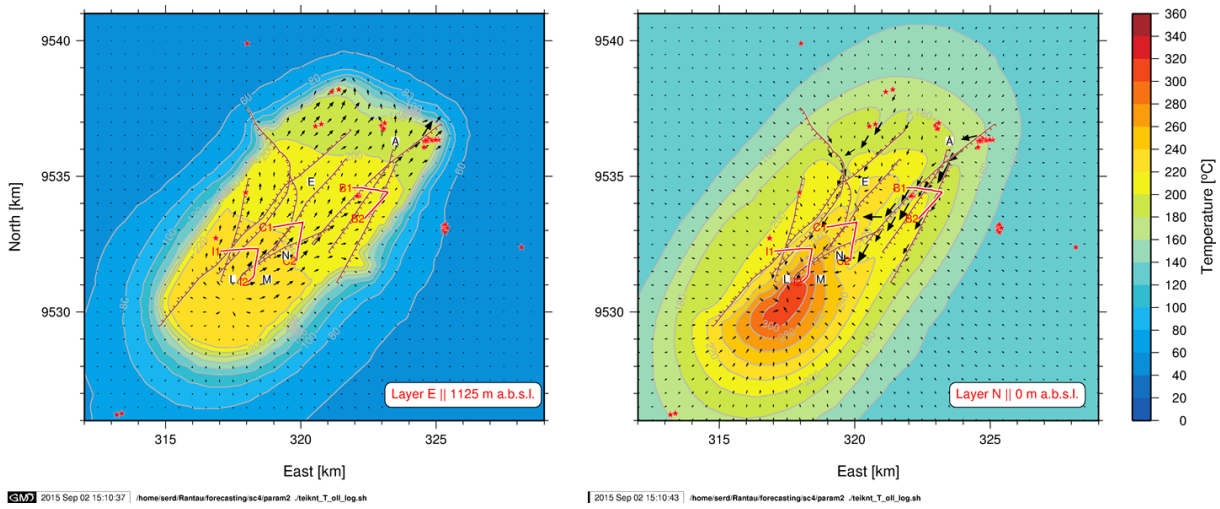

Figure 9: Model temperature distribution in layers E (left) and N (right)

In layer E, the ascending hot fluid is clearly emerging from the Southwest of RD-I2, just above the deep upflow elements, via the high vertical permeability fault FLT30. The fluid then advances primarily to the North and Northeast (particularly through faults FLT30 and FLT 44) where it is eventually consumed by the four mass sinks defined there.

In layer N, fluid is seeping in from the model outer boundaries toward the hot upflow zone of 300°C or more. Faults are primary fluid conduits again (in particular faults FLT 44 and FLT99). This horizontal inflow toward the high enthalpy upflow mixes and results in the 270-300°C water temperature of well RD-I2. Interestingly, it can be observed that very minor cold flow is coming from the North-Northwest to reduce the temperature in the bottom part of RD-C1 and RD-I1. As mentioned before, this is the main flaw of the current model which will need to be revisited once more surface and wells data are available in this area.

The planar pressure distribution in the upper part (layer E) and the lower part (layer N) of the reservoir is shown in Figure 10. In layer E, a pressure high exists above the upflow zone. Lateral flow takes place toward the North and Northeast, where the four mass sinks in layer D reduce their host element pressures and thereby consume fluid mass out of the model. Layer N, on the other hand, shows a pressure low at the upflow zone. This behavior is exactly as expected from the pressure profile of well RD-I2 (Figure 2) and triggers the deep cold recharge from the Northeast boundary as discussed already.

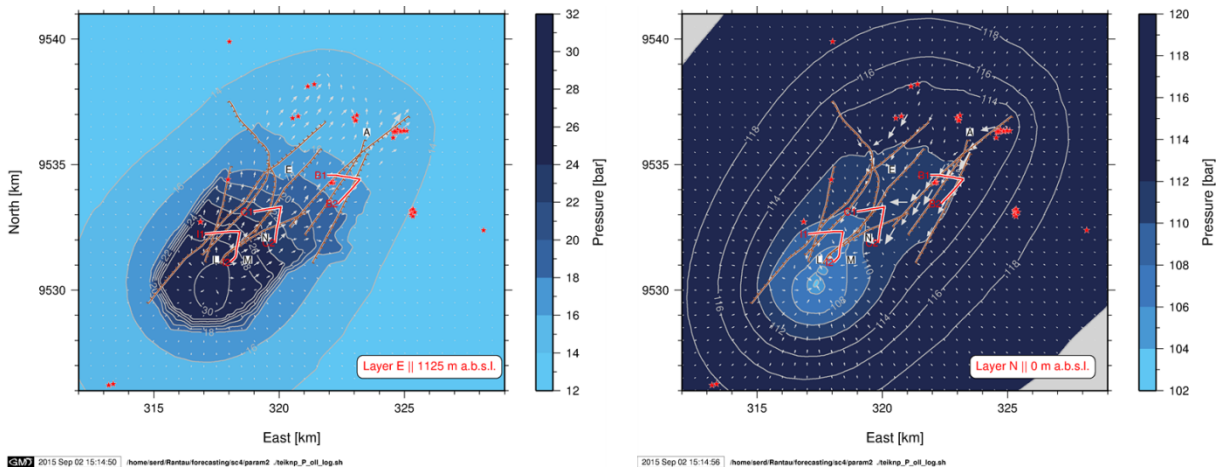

Figure 10: Model pressure distribution in layers E (left) and N (right)

5.3.2 Pressure drawdowns

As discussed earlier, pressure drawdowns at each feed zone during production periods were attempted to be reproduced by the model. A general approximation for the observation data was made by assuming that the well pressure changes instantaneously either when discharged or shut-in. Exception is well I2, which flows under two different regimes: initially, the well flows at medium enthalpy with a low downhole pressure drawdown (nearly 0 bar), while it later flows at higher enthalpy as boiling of the deep feed zones occurs with a resulting high downhole pressure drawdown (about 17 bar). In this particular case, the transition between the two pressure drawdown regimes is assumed to be linear during the course of the well discharge (Figure 11, right plot).

Figure 11 presents the match of the pressure drawdown for the bottom feed zone of well RD-B1 (hit by the main fault FLT44) and the bottom feed zone of well RD-I2 (impacted by sudden boiling). It can be seen that the match is very good, bearing in mind that the model computes the average drawdown of the elements (necessarily lower than the true drawdown at the wellbores). In particular, the pressure drawdown evolution of RD-I2 is properly captured, dictating the low horizontal permeability found by inversion (with high sensitivity) for the bottom part of fault FLT30.

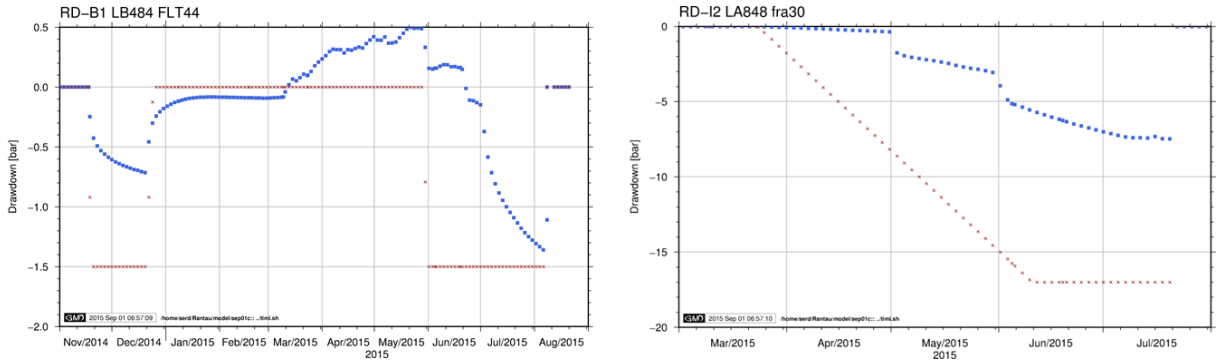

Figure 11: Modeled (blue) and estimated (red) pressure drawdown in wells RD-B1 (left) and RD-I2 (right)

The downhole pressure changes recorded in observation wells RD-I1 and RD-C1 during the interference tests were nearly zero as discussed before. For either well, the model is showing 0.1 to 0.3 bar pressure changes which is close to the accuracy of the measurements. In general the model values are showing slight pressure recovery, thus inferring that the computed pressure signal is mostly coming from these wells recovering from their own discharge rather than from real interference.

5.3.3 Production enthalpies

Production enthalpies of B and C wells are fairly constant over time and excellently matched, except for RD-C1 whose modeled enthalpy is slightly overestimated since the temperature reversal of this well is not properly captured by the model as discussed earlier.

Of particular interest is the production enthalpy of RD-I1 and RD-I2. For the latter, the enthalpy kicked (from 1000 to 1350 kJ/kg) after some time due to the sudden boiling of its deeper feed zones. As can be seen on Figure 12 (right plot), the global trend was captured by the model thanks to the split of fault FLT30 into a top part with high horizontal permeability and a bottom part with low one. However, the enthalpy does not stabilize exactly at the correct values, presenting a misfit of about 100 to 200 kJ/kg. Improvement could certainly be brought with a better description of the structural features in this area, as two separate faults could actually be hit by this well.

In the case of RD-I1 (Figure 12, left plot), the enthalpy rose as the well had to be throttled several times. This presumably reduced the contribution of the deep and colder feed zones of the well at higher wellhead pressures. Therefore, the production history of each feed zone was modified accordingly (discussed earlier) and the inverse calibration apparently did a good job in matching these enthalpy data. However, like for RD-C1 case, the base enthalpy of 1200 kJ/kg measured at fully open conditions is significantly overestimated (about 200 kJ/kg) since the strong temperature reversal of this well is not properly captured by the model.

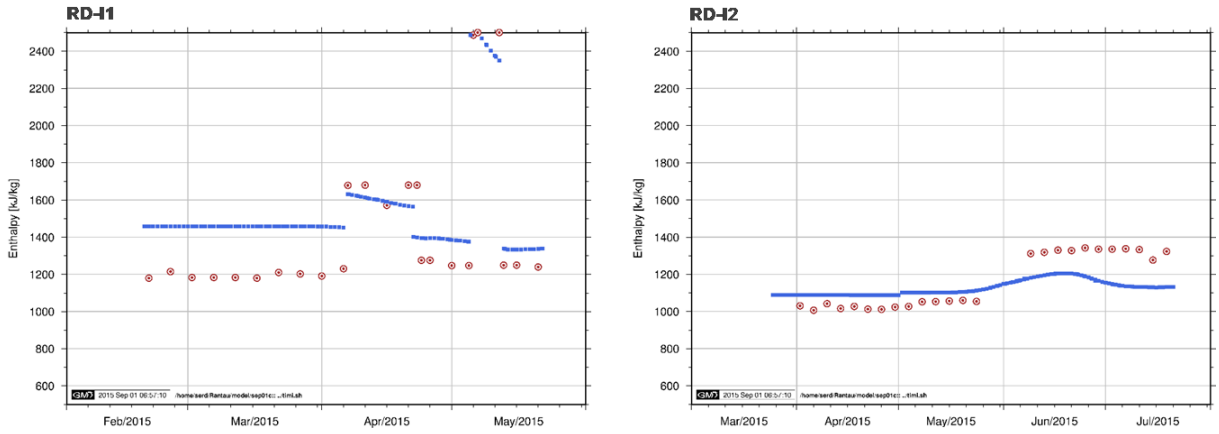

Figure 12: Modeled (blue) and estimated (red) production enthalpy in wells RD-I1 (left) and RD-I2 (right)

6. CONCLUSION

Based on surface data and six deep exploration wells, a comprehensive numerical reservoir model has been built and calibrated in about one and a half months. With a 50x50 km area and about 2 km thickness, this model is able to capture most of the features of the conceptual model that depicts a large and high temperature reservoir strongly controlled by SW-NE striking faults at depth. Accordingly, the model follows a single porosity approach where the near vertical faults are explicitly defined at their true locations and with their own properties. The model has limited thickness and extent to the West, tight lateral boundaries, and can therefore be regarded as conservative which is essential when assessing the production capacity of a field in its early life.

Inverse modeling was used to automatically calibrate the model and achieve the best possible match of the measured data. 36 parameters were inverted for at maximum, most of them being the horizontal and vertical permeabilities of the faults and rocks defined in the model, and the characteristics (rate and possibly enthalpy) of the deep upflow and surface outflow. A total of 1397 observations discretized in space and time and carefully allocated to the correct model elements were used to constrain the inversion.

During the course of the inverse calibration, the distribution of the different faults and rocks was fine-tuned several times to improve the match. The final results of the inversion are very consistent with the conceptual model, with a high enthalpy deep upflow connected to a wide and permeable shallow outflow through a few high permeability faults hosted at depth by a tight matrix. The inversion also reproduces the tight cap rock preventing any infiltration from the overlaying perched aquifer into the geothermal reservoir. The resulting match of the observed data is satisfactory, except for wells RD-C1 and RD-I1 on the northwestern side whose temperature reversals are not reproduced properly by the model. This misfit highlights the necessity to improve the faults description in the West and Southwest parts of the field by acquiring more structural data.

The model calibration being completed, sensitivity runs (not presented in this paper) prove its robustness. The model was then used to carry out several production forecasts in order to establish the field capacity and optimize the production and reinjection scheme for the coming 30 years of operation.

REFERENCES

O'Sullivan, M.J., Pruess, K., and Lippmann M.J.: Geothermal Reservoir Simulation: the State-of-Practice and Emerging Trends, *Proceedings,* World Geothermal Congress, Kyushu – Tohoku, Japan (2000).

Finsterle, S., Pruess, K., Bullivant D.P., and O'Sullivan, M. J.: Application of Inverse Modeling to Geothermal Reservoir Simulation, *Proceedings,* 22nd Workshop on Geothermal Reservoir Engineering, Stanford University, Stanford, CA (1997).

Finsterle, S., and Pruess, K.: Automatic Calibration of Geothermal Reservoir Models Through Parallel Computing on a Workstation Cluster, *Proceedings,* 24th Workshop on Geothermal Reservoir Engineering, Stanford University, Stanford, CA (1999).

Bjornsson, G., and Arnaldsson, A.: Managing Large Geothermal Reservoir Models Under the iTOUGH2 Platform, *Proceedings,* TOUGH Symposium, Lawrence Berkeley National Laboratory, Berkeley, CA (2015).

Finsterle, S.: iTOUGH2 User's Guide, Lawrence Berkeley National Laboratory, Berkeley, CA (2007).